Magnesium Technology 2012
Edited by: Suveen N. Mathaudhu, Wim H. Sillekens, Neale R. Neelameggham, and Norbert Hort
TMS (The Minerals, Metals & Materials Society), 2012

PHASE FIELD MODELING OF β_1 PRECIPITATION IN WE54 ALLOY

Y. Gao[1]; H. Liu[2]; R. Shi[1]; N. Zhou[1]; Z. Xu[2]; J.F. Nie[2]; Y. Wang[1,*]

[1]*The Ohio State University, 477 Watts, 2041 College Road, Columbus, OH 43210, United States*
[2]*Department of Materials Engineering, Monash University, Victoria 3800, Australia*

Keywords: Magnesium alloys, Precipitation, Elastic interaction, Phase field modeling, Precipitation hardening

Abstract

WE54 (Mg-5wt%Y-2wt%Nd-2wt%HRE), which has high strength and lightweight at elevated temperatures, has been identified as one of the most successful magnesium alloys. The strength of WE54 can be achieved via precipitation strengthening by aging at 150~250°C during which precipitations of intermediate phases β_1 and β' and equilibrium phase β take place. In order to understand the microstructure evolution of β_1 phase and its effects on dislocation gliding, a phase field model of β_1 precipitation has been developed. Model inputs, including lattice parameters, precipitate-matrix orientation relationship, elastic constants and free energy data, are obtained from experimental characterization, *ab initio* calculations and thermodynamic databases. Through computer simulations, the equilibrium shape and spatial distribution of the β_1 precipitates are quantitatively determined. The interactions between precipitates and gliding basal dislocations and corresponding effects on the strength of the alloy have been investigated.

1. Introduction

With high strength to weight ratio, magnesium alloys have been widely used for applications in aerospace and automotive industries [1-13]. One of the most successful commercial magnesium alloys developed for fabricating component is WE54, which has a composition of about 5wt% Y, 2wt%Nd and 2wt% heavy rare-earth elements. WE54 alloy has a tensile strength of 200MPa, improved corrosion resistance and excellent retention of properties at elevated temperatures up to 300°C [14-17]. The strength of the WE54 alloy is achieved via precipitation hardening. Intermediate phases of β_1, β' and equilibrium phase of β form when the alloy is heat treated in the T6 condition (solution treatment for 8 h at 525°C, a hot water quench and a subsequent aging treatment of 16 h at 250°C). Previous studies have shown that β_1 precipitates have a plate shape with $\{1\bar{1}00\}$ habit planes and eventually convert into β phase during prolonged ageing. Interesting multi-variant microstructures such as a "triadic" structure, which is constructed by three different $\{1\bar{1}00\}$ plates that are rotated by 120° from each other, have been observed in experiments (Fig. 1). In addition, it has also been suggested that these prismatic plates effectively strengthen the alloy by providing barriers to gliding dislocations and highest hardness can be reached by peak-aging [14-17]. Thus great interests have been shown in designing and heat treating high strength magnesium alloys by which the fraction and size of precipitates can be controlled [2, 3]. In this paper, effects of β_1 precipitates on the yield stress of WE54 are investigated by computation and simulation method. The multi-variant morphology of β_1 precipitates and formation mechanism of triadic structure will be discussed in a separate paper.

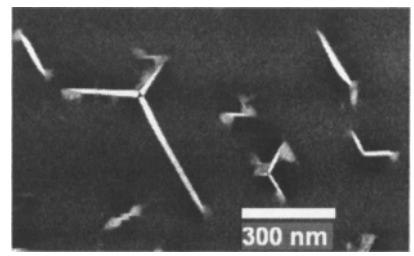

Fig. 1. Microstructure of WE54 in T6 condition

Phase field modeling and simulation have been used widely to treat both diffussional and diffussionless phase transformations and dislocation-precipitate interactions [18-23]. In this study we formulate a phase field model to study the morphology of β_1 and the interaction between β_1 and gliding basal dislocations. In particular, we document through systematic computer simulations (a) the equilibrium shape and spatial distribution of β_1 precipitates, (b) effects of β_1 precipitates on gliding basal dislocations and corresponding critical resolved shear stress.

The stress fields surrounding a single β_1 precipitate are determined by the interplay between chemical free energy and elastic strain energy. The chemical free energy model for the matrix and precipitate phases in WE54 alloy are formulated from existing thermodynamics databases [24]. The elastic strain energy is formulated using Khachaturyan and Shatalov's microelasticity theory [25, 26]. In order to study the interaction between β_1 precipitates and dislocation, a simplified model based on Orowan bowing mechanism is proposed and benchmarked against phase field calculations to achieve higher efficiency for parametric studies of the influence on deformation behavior from different factors such as resolved shear stress, volume fraction and size of β_1 precipitates.

In the following sections, thermodynamic modeling and transformation strain calculation are first presented (Section 2 and 3), followed by descriptions of the phase field model (Section 4). Simulation results are presented and discussed respectively in Section 5 and 6. The major findings are summarized in Section 7.

2. Thermodynamic Modeling of HCP Phase in WE54

The accuracy of phase field simulations and predictions relies on the accuracy of available thermodynamic databases, especially the free energy of the HCP matrix phase in the case of WE54. In this study, the composition of WE54 is taken as Mg-5wt%Y-4wt%Nd,

and the chemical free energy of which can be described by a sub-regular solution model [24]:

$$\begin{aligned} G^{HCP}(x_{Mg},x_Y,x_{Nd}) &= x_{Mg}G_0^{Mg} + x_Y G_0^Y \\ &+ x_{Nd}G_0^{Nd} RT(x_{Mg}\ln x_{Mg} + x_{Mg}\ln x_Y + x_{Nd}\ln x_{Nd}) \\ &+ x_{Mg}x_Y\sum_i L'_{Mg,Y}(x_{Mg}-x_Y)^i \\ &+ x_{Mg}x_{Nd}\sum_i L'_{Mg,Y}(x_{Mg}-x_{Nd})^i \\ &+ x_{Nd}x_Y\sum_i L'_{Nd,Y}(x_{Nd}-x_Y)^i \end{aligned} \quad (1)$$

where x_{Mg}, x_Y, x_{Nd} are mole fraction of each species respectively.

3. Crystallography of HCP to β_1 Transformation

3.1 Crystallography Of β_1 Phase And Its Orientation Relationship With HCP Matrix

The β_1 phase has a cubic structure with a = 0.741nm, which has a $Fm\bar{3}m$ space group. It is an ordered phase with a stoichiometry of $Mg_3(Y,Nd)_1$. The crystal structure of β_1 is shown in Fig. 2. It can be considered as a BCC lattice if different atoms are not distinguished. Furthermore, a FCC sub-lattice of (Y/Nd) atoms can be found within the BCC structure and the other lattice sites have been occupied by Mg atoms which gives a stoichiometry of $Mg_3(Y,Nd)_1$.

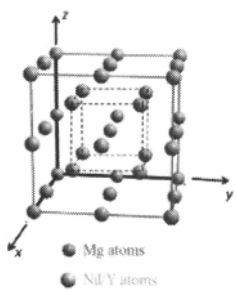

Fig. 2. Crystal structure of β_1 phase

According to experimental observations, the lattice correspondence between β_1 and HCP Mg (a_{HCP} = 0.321 nm, c_{HCP} = 0.521 nm) matrix is as follows which was used in the calculation of transformation matrix [17]:

$$[0001]_{HCP} \rightarrow \frac{1}{2}[110]_{\beta_1} \qquad \frac{2}{3}[1\bar{1}20]_{HCP} \rightarrow \frac{1}{2}[\bar{1}\bar{1}1]_{\beta_1},$$
$$2[\bar{1}100]_{HCP} \rightarrow \frac{1}{2}[\bar{1}13]_{\beta_1}$$

3.2 Calculation Of Stress-Free Transformation Strain (SFTS)

Since prismatic plates of β_1 precipitates have been observed in experiments, it is more convenient to focus our study on the $(0001)_{HCP}$ plane by which calculations can be greatly simplified. Our coordinate system is constructed as Fig. 3, in which $[\bar{1}100]_{HCP}$ and $[11\bar{2}0]_{HCP}$ are set as x and y directions respectively.

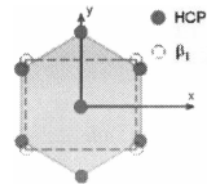

Fig. 3. 2D Sketch of structure transition from HCP to β_1

Because $[0001]_{HCP}$ has 3-fold symmetry while $[110]_{\beta_1}$ has only 2-fold symmetry, three kinds of different β_1 variants will be generated during the transformation [16, 17]. The transformation matrix and transformation strain of β_1 variants have been calculated as follows:

$$U_2 = \begin{bmatrix} \frac{\sqrt{2}a_{\beta_1}}{2\sqrt{3}a_{HCP}} & 0 \\ 0 & \frac{a_{\beta_1}}{2a_{HCP}} \end{bmatrix} = \begin{bmatrix} 0.942 & 0 \\ 0 & 1.154 \end{bmatrix} \quad (2)$$
$$U_1 = R^T U_2 R = \begin{bmatrix} 1.102 & 0.092 \\ 0.092 & 0.995 \end{bmatrix}$$
$$U_3 = R U_2 R^T = \begin{bmatrix} 1.102 & -0.092 \\ -0.092 & 0.995 \end{bmatrix}$$
$$\varepsilon(p) = \frac{U_p^T U_p - I}{2}, \quad p = 1 \sim 3$$

where R is a rotation matrix of 120 degree, U_p and $\varepsilon(p)$ are the transformation matrix and stress-free transformation strain of variant p respectively.

$$R = \begin{bmatrix} \cos 120^\circ & \sin 120^\circ \\ -\sin 120^\circ & \cos 120^\circ \end{bmatrix} \quad (3)$$

4. Phase Field Model

4.1. Energy Formulation For HCP ->β_1 Transition

According to Landau's theory of phase transformations, a set of 3 order parameters, $\{\eta_1, \eta_2, \eta_3\}$ has been introduced to characterize the HCP to β_1 transformation, with $\eta_1=\eta_2=\eta_3=0$ representing the HCP phase and $\{\eta_i = 1, \eta_{j\neq i} = 0\}$ (where i=1~3 and j=1~3) representing the 3 variants of β_1 phase. In addition, an interpolation function $h(\eta_i) = \eta_i^3(10 - 15\eta_i + 6\eta_i^2)$ is used to connect the equilibrium free energy of the two phases through the order parameters. The final form of the chemical free energy density in the phase field model can be expressed as a function of five field variables (unit: J/m^3):

$$\begin{aligned} &f(x_Y, x_{Nd}, \{\eta_p, p = 1 \sim 3\}) \\ &= V_m^{-1}\left[\begin{array}{l} G_{HCP}\cdot(1 - \sum_{p=1}^{3} h(\eta_p)) \\ + G_{\beta 1}\cdot\sum_{p=1}^{3} h(\eta_p) + \theta\sum_{p=1}^{3}\sum_{q=1}^{3}\eta_p^2\eta_q^2 \end{array}\right] \end{aligned} \quad (4)$$

In Equation(4), V_m is the molar volume and G_{HCP} and $G_{\beta 1}$ are the equilibrium Gibbs free energy of the HCP matrix and β_1 phase, respectively. θ is the coefficient to describe anti-phase boundary energy. G_{HCP} at 523K is fitted from the available thermodynamic data (see Section 2) (in a unit of 10^4J/mol)

$$G_{HCP} = -1.8989 - 5.1124x_Y - 4.7448x_{Nd} + 6.8855x_Y^2 + 4.1893x_Y x_{Nd} + 8.2346x_{Nd} \quad (5)$$

and $G_{\beta 1}$ is approximated as a second order function of Ni, Pt compositions.

$$G_{\beta 1} = -1.6803 - 6.7795x_Y - 6.4223x_{Nd} + 4.0x_Y^2 + 6x_Y x_{Nd} + 4.0x_{Nd}^2 \quad (6)$$

where the constants are determined (a) by a common tangent plane going through the equilibrium HCP matrix concentration and the equilibrium β_1 phase concentration determined from experimental characterization and (b) considering the effect of the curvature of the parabola on the interfacial energy between the two phases. For an alloy of $Mg_{97.81}Y_{1.47}Nd_{0.72}$, the equilibrium Y and Nd concentrations determined by the common tangent construction are x_Y(HCP)=0.0075, x_{Nd}(HCP)=0.001 and $x_Y(\beta_1)$=0.1373, $x_{Nd}(\beta_1)$=0.1127, which are close to the equilibrium concentrations determined by experiment at 523 K.

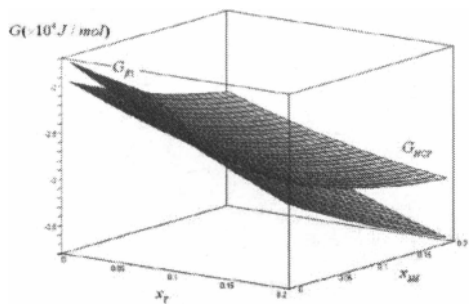

Fig. 4. Free energy plot of HCP phase and β_1 phase

Assuming the lattice misfit between the two coexisting phases is only associated with structural non-uniformities, the SFTS field is formulated as a function of structural order parameters:

$$\varepsilon_{ij}^T(r) = \sum_{p=1}^{3} \varepsilon_{ij}(p) h(\eta_p) \quad (7)$$

The total elastic energy can be formulated following Khachaturyan-Shatalov's microelasticity theory [26]:

$$E_{elastic} = \frac{1}{2} \sum_{p,q=1}^{3} \int \frac{d^3k}{(2\pi)^3} B_{pq}(\vec{n}) \{\tilde{\eta}_p\}_k \{\tilde{\eta}_q\}_k^* \quad (8)$$

where the integral is taken in the reciprocal space, and $\vec{n}$ is a unit vector in the reciprocal space. Note that $\vec{k} = 0$ is to be excluded, which defines the principle value of the integration. $\{\tilde{\eta}_p\}_k$ is the Fourier transform of η which is a function of spatial coordinates. The superscript asterisk indicates the complex conjugate. $B_{pq}(\vec{n})$ is the integral coefficient determined by the Fourier transform of the Green function of anisotropic elasticity [26].

After incorporating the gradient terms, the total free energy of the system becomes:

$$F = \int d^3r \cdot \left[\begin{array}{l} f(x_Y, x_{Nd}, \{\eta_p\}) + \frac{K_Y}{2}(\nabla x_Y)^2 \\ + \frac{K_{Nd}}{2}(\nabla x_{Nd})^2 + \sum_{p=1}^{3} \frac{K_\eta}{2}(\nabla \eta_p)^2 \end{array} \right] + E_{elastic} \quad (9)$$

4.2. Kinetic Equations For HCP -> β_1 Transition

The Cahn-Hilliard equation and Allen-Cahn equation are used to describe the time evolution of the concentration and order parameter fields

$$\frac{1}{V_m^2}\frac{\partial x_Y}{\partial t} = \nabla\left\{ M_Y \nabla\left[\frac{\delta F}{\delta x_Y} \right] \right\} \quad (10a)$$

$$\frac{1}{V_m^2}\frac{\partial x_{Nd}}{\partial t} = \nabla\left\{ M_{Nd} \nabla\left[\frac{\delta F}{\delta x_{Nd}} \right] \right\} \quad (10b)$$

$$\frac{\partial \eta_p}{\partial t} = -L\frac{\delta F}{\delta \eta_p}, p = 1 \sim 3 \quad (10c)$$

where x_Y, x_{Nd} are the molar concentrations of Y and Nd, M_Y and M_{Nd} are the chemical mobilities and L is the kinetic coefficient for the time-evolution of the order parameters.

4.3 Phase Field Analysis Based Orowan Bowing

A line tension based Orowan bowing mechanism [27] has been used as the basis to provide an analysis on the interaction between precipitation and dislocation. The line tension of the dislocation is assumed to be

$$T = \frac{\alpha \mu b^2}{2} \quad (11)$$

Where μ is the shear modules, b is Burger vector and α is a constant whose typical value is 1 to 2. Thus the critical resolved shear stress caused by precipitation hardening can be determined by Orowan's Equation [27],

$$\tau_{crss} = \frac{\alpha \mu b}{\lambda} \quad (12)$$

Where λ is the interparticle spacing and the yield stress can be calculated,

$$\sigma_y = \frac{\tau_{crss}}{\gamma} + \sigma_y^0 \tag{13}$$

Where γ is Schmid factor and σ_y^0 is the yield stress of material without precipitation which is caused by many factors such as lattice friction and solute drag.

A non-conserved field variable ξ is introduced to define two states: ξ=1 represents that the materials have been sheared by the dislocation while $\xi = 0$ means the non-sheared materials. A double well free energy function is used to confine the phase variable within the vicinity of either 0 or 1.

$$g(\xi) = A\xi^2(1-\xi)^2 \tag{14}$$

Since the phase variable is defined as the displacement field, the dislocation line is interpreted as the boundary of the displaced region where $\xi = 1$. Gradient term should be added to total energy formulation and the equilibrium phase variable profile is determined by the balance between double-well potential and gradient energy which is corresponding to the line tension of the dislocation in this case. The total free energy can be written as:

$$G = \int d^3r \left[g(\xi) + Bx_\gamma \xi + \frac{\kappa_\xi}{2}(\nabla\xi)^2 - H\xi \right] \tag{15}$$

Where $H\xi$ is the external work term. $Bx_\gamma\xi$ is the extra energy penalty for cutting β_1. The concentration field x_γ is used to define spatial distribution of β_1 precipitates in HCP matrix. By fitting Anti-phase boundary (APB) energy, the numerical value of parameter B can be obtained. In our simulation, a sufficient large value of B has been chosen to prevent APB cutting. The scaling factor between H and real applied shear stress has been determined by comparing simulated critical stress H^* with the analytical result in Equation (12).

The kinetic equation of displacement field is Ginzburg-Landau type:

$$\frac{\partial\xi}{\partial t} = -L_\xi \frac{\delta G}{\delta \xi} \tag{16}$$

Where L_ξ is the kinetic coefficient (dislocation mobility).

5. Simulation Results

By simplification, the interfaces between HCP matrix and β_1 precipitates are considered as coherent, and the interfacial energy is assumed to be 50 mJ/m^2, which yields a grid size of l_0=0.424 *nm* in the phase field simulation. Thus, a computation cell of 512 grids represents a physical system of edge length 217 *nm*. The elastic constants used in the simulations are [28]: c_{11}=63.5*GPa*, c_{12}=24.85*GPa*, c_{44}=19.3*GPa*, c_{13}=20.0*GPa*, c_{33}=66*GPa*.

5.1 Equilibrium Shape Of A β_1 Precipitate

The equilibrium shape of an isolated β_1 precipitate (variant 1) obtained from the simulation is shown in Fig. 5. It has a plate-shape with $(1\bar{1}00)$ habit plane. Moreover, rim of the plate, which is corresponding to two tips in 2D, is slightly distorted because of elastic interaction. Based on experimental observations, due to the coexisting of β' precipitates at tips of β_1 plates which reduces stress concentration, single β_1 plate cannot be found in WE54 alloy. However, single β_1 plate with slightly distorted tips can be observed in Mg-Nd binary system which agrees with our simulation results.

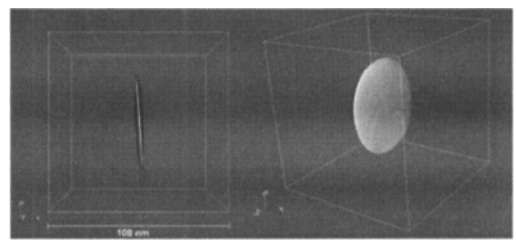

Fig. 5. 3D simulation results of a single β_1 particle

5.2 Multi-particle Correlation

In this study, the Langevin noise terms are used to generate microstructures consisting of the multi-particles in the simulations. An example is shown in Fig. 6. Three $\{1\bar{1}00\}$ habit planes can be obtained which form a triadic structure. It can be showed that there is a triangle of HCP matrix in the center of a star due to elastic interaction which agrees with experimental observations.

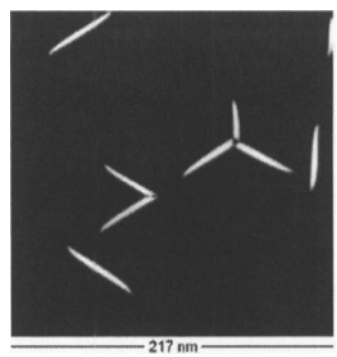

Fig. 6. Simulation results of multi-particle generated by langevin noise terms

5.3 Interaction Between Precipitation And Dislocation

A typical microstructure generated by simulations has been used to study the hardening effect of β_1 phase. The shear modules used is μ= 18.5GPa [28], and the coefficient α in Equation (11) is taken as 1. In Fig. 7, a slip system of $\{0001\}<11\bar{2}0>$ is considered under applied shear stress (50MPa).

Initially, a screw type of dislocation is put into the left side of the system. Due to the blockage of β_1 precipitates, some part of the dislocation line has already been bowed under the applied external stress and it becomes mixed type. By assuming the typical yield stress without precipitation is ~130MPa and Schmid factor γ=0.5, this stress level is corresponding to 230 MPa uniaxial stress. Finally, the dislocation line has gone through the microstructure

and dislocation loops around uncuttable β_1 particles can be observed finally.

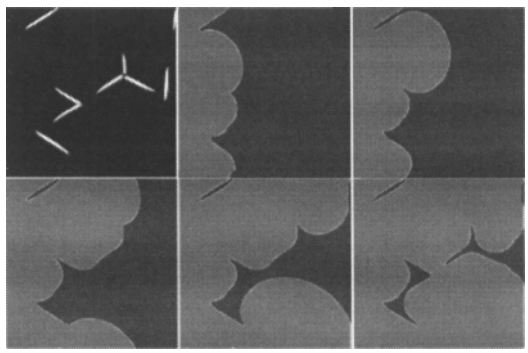

Fig. 7. Displacement field increase under 50MPa shear stress

6. Discussions

6.1 Habit plane of β_1 particle

Since the SFTS of β_1 phase is relatively large comparing with most other diffusional transitions, the shape of an equilibrium β_1 particle is almost determined by elastic interaction. According to the elastic energy formulation, habit plane n_p of β_1 variant $p$can be determined by finding the minimum point of $B_{pp}(\vec{n})$ function, which is corresponding to a direction in reciprocal space and a plane normal in real space [26].

$$\left.\frac{\partial B_{pp}(\vec{n})}{\partial \vec{n}}\right|_{n=n_p} = 0, \quad p = 1 \sim 3 \tag{17}$$

By solving above equations, habit planes for different variants can be figured out:

$$n_1 = \begin{bmatrix}1\\0\\0\end{bmatrix}, \begin{bmatrix}0.5\\0.866\\0\end{bmatrix}; n_2 = \begin{bmatrix}-0.5\\0.866\\0\end{bmatrix}, \begin{bmatrix}0.5\\0.866\\0\end{bmatrix};$$
$$n_3 = \begin{bmatrix}-0.5\\0.866\\0\end{bmatrix}, \begin{bmatrix}1\\0\\0\end{bmatrix} \tag{18a}$$

Considering the coordinate system we constructed, the three habit planes above belong to $\{1\bar{1}00\}_{HCP}$ which are consistent with experimental observations. Moreover, since two different habit planes could be formed by each variant, one habit plane is corresponding to one of two possible β_1 variants. Totally, there are six different kinds of β_1 plates based on the analysis of crystallography.

6.2 Effects Of β_1 Precipitates On Yield Stress

By precipitation hardening, high yield stress of Mg-Y-Nd system can be achieved via aging treatment. Based on the mechanism of Orowan bowing, yield stress is greatly influenced by volume fraction and particle size of precipitation. In order to find the relation quantitatively, computation method could be more efficient both timely and economically comparing with experimental efforts.

A series of simulations have been designed with different initial composition and nucleation rate which gives various microstructure with different precipitate fraction and particle size distribution. The critical resolved shear stress and yield stress for different microstructure have been calculated by simulations. The relationship between yield stress and volume fraction and average particle size of precipitates has been quantified by linear fitting which is showed in Fig. 8.

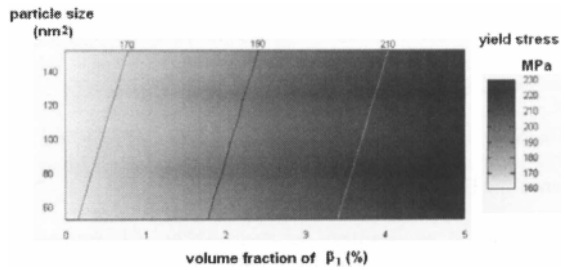

Fig. 8. Yield stress as a function of volume fraction and size of β_1

An empirical function for yield stress is as follows,

$$\sigma_y(MPa) = 172 + 12.3 \times Vf(\%) - 0.078 \times Pz(nm^2) \tag{19}$$

Where Vf is volume fraction of β_1 and Pz is particle size which is measured as the area in (0001) cross-section.

From Equation (19), it can be concluded that yield stress increase with volume fraction and decrease with particle size. In order to get high yield stress alloy, we should increase volume fraction of β_1 and decrease particle size. In experiments, change of volume fraction can be achieved by adjusting initial composition, controlling aging time and temperature. And particle size can be controlled by cold working before aging, by which more defects can be introduced as the nucleation sites of β_1 precipitates. Aging time is a subtle parameter because both volume fraction and particle size increase with aging time which makes two opposite contributions to yield stress. As a result, some suggestions to improve yield strength can be concluded based on our analysis: (a) increasing initial chemical composition of Y and Nd (or RE) which results in the increase of equilibrium β_1 fraction; (b) moderate cold working which increases the nucleation rate of β_1 precipitates; (c) controlling aging temperature and time properly.

7. Summary

A phase field model which describes the precipitation of β_1 in WE54 alloy has been developed. The main principal transformation strain of β_1 is found to be -5.6%, +16.7% and +0.6%. If the slight mismatch in the third dimension is ignored, an invariant plane can be achieved between β_1 phase and HCP matrix which are corresponding to $\{1\bar{1}00\}_{HCP}$ plane. The plate-like shape of a β_1 particle is determined by the interplay of interfacial energy and elastic energy.

Based on Orowan bowing, a phase field analysis has been applied to investigate the interaction between β_1 precipitates and gliding basal dislocation. An empirical function has been proposed to predict the yield stress based on the statistical data of volume fraction and particle size of precipitates in simulations. Yield stress will increase with volume fraction and decrease with particle size of β_1 precipitates. In order to get higher strength alloy, an increase in the Y, Nd (RE) concentrations, the moderate cold working and the proper aging temperature and time control are suggested.

Reference

1. Agnew, S.R. and J.F. Nie, *Preface to the viewpoint set on: The current state of magnesium alloy science and technology.* Scripta Materialia, 2010. **63**(7): p. 671-673.

2. He, S.M., et al., *Microstructure evolution in a Mg-15Gd-0.5Zr (wt.%) alloy during isothermal aging at 250 degrees C.* Materials Science and Engineering A 2006. **431**(1-2): p. 322-327.

3. Hono, K., et al., *Towards the development of heat-treatable high-strength wrought Mg alloys.* Scripta Materialia, 2010. **63**(7): p. 710-715.

4. Jayaraj, J., et al., *Enhanced precipitation hardening of Mg-Ca alloy by Al addition.* Scripta Materialia, 2010. **63**(8): p. 831-834.

5. Mendis, C., et al., *Effects of Ca additions on microstructures, age hardening response and creep behaviour of Mg-8Zn-4Al casting alloy.* Magnesium Technology 2003, 2003: p. 183-188.

6. Mendis, C.L., et al., *Precipitation of prismatic plates in Mg-0.3Ca alloys with In additions.* Scripta Materialia, 2011. **64**(2): p. 137-140.

7. Meng, J., et al., *Effect of Y for enhanced age hardening response and mechanical properties of Mg-Gd-Y-Zr alloys.* Materials Science and Engineering A 2007. **456**(1-2): p. 78-84.

8. Nie, J.F., X. Gao, and S.M. Zhu, *Enhanced age hardening response and creep resistance of Mg-Gd alloys containing Zn.* Scripta Materialia, 2005. **53**(9): p. 1049-1053.

9. Nie, J.F., et al., *Enhanced age-hardening response of Mg-Zn alloys via Co additions.* Scripta Materialia, 2011. **64**(6): p. 506-509.

10. Nie, J.F. and B.C. Muddle, *On the form of the age-hardening response in high strength aluminium alloys.* Materials Science and Engineering A 2001. **319**: p. 448-451.

11. Nie, J.F., Y.M. Zhu, and A.J. Morton, *Improvement in the age-hardening response of Mg-Y-Zn alloys by Ag additions.* Scripta Materialia, 2008. **58**(7): p. 525-528.

12. Oh-ishi, K., et al., *Age-hardening response of Mg-0.3 at.%Ca alloys with different Zn contents.* Materials Science and Engineering A 2009. **526**(1-2): p. 177-184.

13. Ping, D.H., K. Hono, and J.F. Nie, *Atom probe characterization of plate-like precipitates in a Mg-RE-Zn-Zr casting alloy.* Scripta Materialia, 2003. **48**(8): p. 1017-1022.

14. Antion, C., et al., *Hardening precipitation in a Mg-4Y-3RE alloy.* Acta Materialia, 2003. **51**(18): p. 5335-5348.

15. Antion, C., et al., *Early stages of precipitation and microstructure control in Mg-rare earth alloys.* Philosophical Magazine, 2006. **86**(19): p. 2797-2810.

16. Nie, J.F. and B.C. Muddle, *Precipitation in magnesium alloy WE54 during isothermal ageing at 250 degrees C.* Scripta Materialia, 1999. **40**(10): p. 1089-1094.

17. Nie, J.F. and B.C. Muddle, *Characterisation of strengthening precipitate phases in a Mg-Y-Nd alloy.* Acta Materialia, 2000. **48**(8): p. 1691-1703.

18. Wang YZ, C.L., *Simulation of microstructural evolution using phase field method.* Methods in materials research, ed. Kaufmann. 2000, New York: Wiley.

19. Steinbach, I., *Phase-field models in materials science.* Modelling and Simulation in Materials Science and Engineering, 2009. **17**(7).

20. Zhou, N., et al., *Phase field modeling of channel dislocation activity and gamma ' rafting in single crystal Ni-Al.* Acta Materialia, 2007. **55**(16): p. 5369-5381.

21. Zhou, N., et al., *Effect of Ni(4)Ti(3) precipitation on martensitic transformation in Ti-Ni.* Acta Materialia, 2010. **58**(20): p. 6685-6694.

22. Wang, Y.Z. and J. Li, *Phase field modeling of defects and deformation.* Acta Materialia, 2010. **58**(4): p. 1212-1235.

23. Zhou, N., et al., *Modeling displacive-diffusional coupled dislocation shearing of gamma ' precipitates in Ni-base superalloys.* Acta Materialia, 2011. **59**(9): p. 3484-3497.

24.Meng. F.G, et al., *Experimental investigation and thermodynamic calculation of phase relations in the Mg-Nd-Y ternary system.* Materials Science and Engineering A 2007. **454**: p. 266-273.

25. Cahn JW, H.J., The Journal of chemical physics, 1958. **28**(2): p. 258-267.

26. Khachaturyan, A., *Theory of Structural Transformations in Solids.* 1983, New York: Wiley.

27. Orowan, E., *Mechanical strength properties and real structure of crystals.* Zeitschrift Fur Kristallographie, 1934. **89**(3/4): p. 327-343.

28. Ganeshan, S., et al., *Effect of alloying elements on the elastic properties of Mg from first-principles calculations.* Acta Materialia, 2009. **57**(13): p. 3876-3884.